2025 IEEE/SICE International Symposium on System Integration (SII)
January 21-24, 2025, Munich, Germany

A Two-Port Network for a Ball-screw Inerter Employing Nonlinearities

Yu-Ren Lin, Chung-Hsien Lee, I-Haur Tsai, Ya-Chun Yu, Jia-Yush Yen, and Fu-Cheng Wang

Abstract— **We propose a two-port representation of the inerter and conduct experiments for verification. Considering the mechanical components and the interactions, the model can successfully forecast the inerter responses during experiments, increasing the fitting accuracy from 49% to 75%. The results show that the two-port network can effectively forecast systems' responses employing the inerter.**

I. Introduction

The inerter ideas were proposed in 2001 [1] to substitute the mass in mechanical systems, such as vehicle suspensions [2, 3], optical tables [4], and seismic absorbers [5]. These systems' performance can be improved passively. The inerter has various realizations, such as the rack and pinion [6], the hydraulic pump [7], the ball-screw [8], and those with electrical motors [4]. Among them, the ball-screw realization is most popular because of its compact design with relatively low friction and backlash [9].

The nonlinear properties of the inerter can affect system responses and degrade system performance. Hence, Wang and Su [8] considered the backlash and friction effects to investigate their impacts on system performance using a nonlinear mechanical network. Sun et al. [10] expanded this nonlinear model by integrating the nut mass while disregarding the backlash effect. Li et al. [11] refined the model by considering the Stribeck effect and the frequency-related friction. Song et al. [12] then combined the constant Coulomb and speed-dependent viscous frictions to simplify the model.

Because the ball-screw inerter has several mechanical components, this paper proposes a two-port network representation to simplify the interactions between mechanical components. Two-port representation can explore a system's internal behavior while capturing its complex structure details. We will introduce a ball-screw inerter and derive its two-port representation in Section II. Section III describes experiments to obtain the model's parameters. Finally, we draw conclusions in Section IV.

II. Nonlinear Network Representation

This section introduces the network realization of a ball-screw inerter (see Fig. 1). Two red plates are the terminals, as shown in Fig. 2, where one terminal is grounded. The yellow disks in Fig. 1(a) are flywheels attached to one end of the ball screw. Two well-lubricated ball splines are applied to strengthen the structure.

We analyze the complex system dynamic equations and propose a mechanical block diagram, as shown in Fig. 3, where f_1, f_B, and f_n are as follows:

$$f_1 = K_{f_1}\left(\dot{x}_B\right), f_{\mathrm{B}} = K_{f_{\mathrm{B}}}\left(\dot{x}_\theta\right), f_n = K_{f_n}\left(\dot{x}_\theta\right), \qquad (1)$$

in which K_{f_1}, K_{f_B}, and K_{f_n} represent the relationships between velocities and frictions, which can stand for any preferred friction model. Separating the blocks using crosses in different colors in Fig. 3, Fig. 4 shows the equivalent two-port representation with the following transfer functions:

$$\begin{aligned}
&N_{M_B} = \begin{bmatrix} \frac{1}{m_B s} & \frac{-1}{m_B s} \\ \frac{1}{m_B s} & \frac{-1}{m_B s} \end{bmatrix}, N_{M_s} = \begin{bmatrix} \frac{1}{m_s s} & \frac{-1}{m_s s} \\ \frac{1}{m_s s} & \frac{-1}{m_s s} \end{bmatrix}, \\
&N_{Q_B} = \begin{bmatrix} Q_B & -Q_B \\ Q_B & -Q_B \end{bmatrix}, N_{Q_n} = \begin{bmatrix} Q_n\cos^2\theta & -Q_n\cos^2\theta \\ Q_n\cos^2\theta & -Q_n\cos^2\theta \end{bmatrix}, \\
&N_{K_{f_1}} = \begin{bmatrix} 0 & 1 \\ 1 & K_{f_1} \end{bmatrix}, N_{K_{f_{nS}}} = \begin{bmatrix} 0 & 1 \\ 1 & K_{f_n}\left(\dot{x}_\theta\right)\sin\theta \end{bmatrix}, \\
&N_{K_{f_B}} = \begin{bmatrix} 0 & 1 \\ 1 & K_{f_B} \end{bmatrix}, N_{K_{f_{nC}}} = \begin{bmatrix} 0 & 1 \\ 1 & K_{f_n}\cos\theta \end{bmatrix}, \Phi = \frac{1}{bs}.
\end{aligned} \qquad (2)$$

where b is the ideal inertance. F is the applied force, and T_B is the stress caused by the deformation across the plate and the ball screw. f_1 is the friction between the first plate and the supporting wood. m_B is the integrated mass of the plate, ball spline nuts, and the bearing. x_B is the plate displacement. T_f is the stress caused by the deformation of the nut and the plate. f_n is the sliding friction inside the ball-screw nut. θ is the

*Research supported by the Ministry of Science and Technology of Taiwan under Grand MOST 111-2221-E-002-190-MY3.

Yu-Ren Lin, Chung-Hsien Lee, and Fu-Cheng Wang are with the Department of Mechanical Engineering in National Taiwan University, Taipei, Taiwan (Tel: +886-2-33662680; e-mail: fcw@ntu.edu.tw, r11522813@ntu.edu.tw, and d10522006@ntu.edu.tw).

I-Haur Tsai is with the Department of Energy and Refrigerating Air-Conditioning Engineering in National Taipei University of Technology, Taipei, Taiwan (e-mail: mr.ihaur@gmail.com).

Ya-Chun Yu is with the Department of Electrical Engineering in National Taiwan University, Taipei, Taiwan (e-mail: b10901122@ntu.edu.tw).

Jia-Yush Yen is with the Department of Mechanical Engineering in National Taiwan University of Science and Technology, Taipei, Taiwan (e-mail: jyen@mail.ntust.edu.tw).

thread angle of the ball-screw. m_s is the combined mass of ball-screw and attached flywheels, and I_s is the integrated moment of inertia. x_s is the linear displacement. f_B is the friction caused by rotation of the bearing. $\theta_s = 2\pi x_s / p$ represents the rotation of the ball-screw, where p is the pitch. Q_B and Q_n represent the stiffness and damping characteristics of the deformation. x_n is the deformation along the direction of motions. Lastly, R in the Fig. 3 is the radius of the ball-screw.

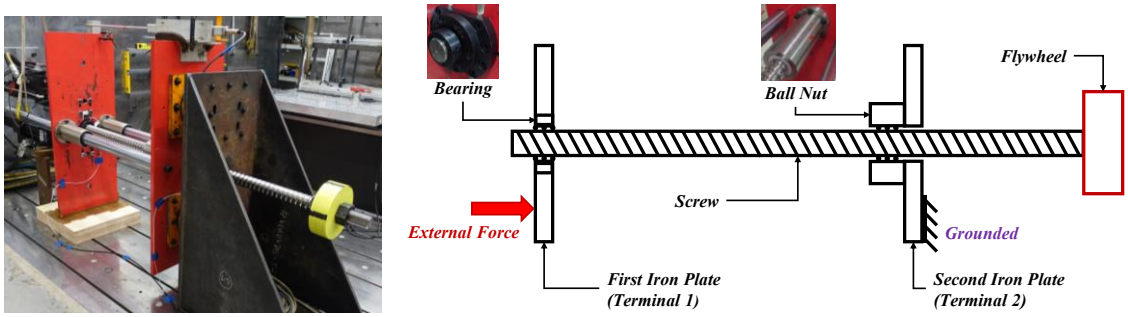

Figure 1. A ball-screw inerter. (a) Realization. (b) Schematic model.

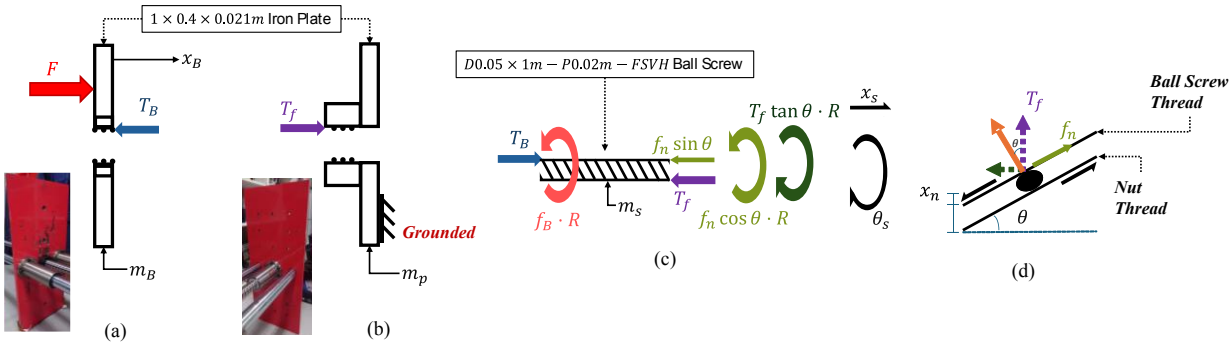

Figure 2. Free body diagram of the component in the ball-screw inerter.

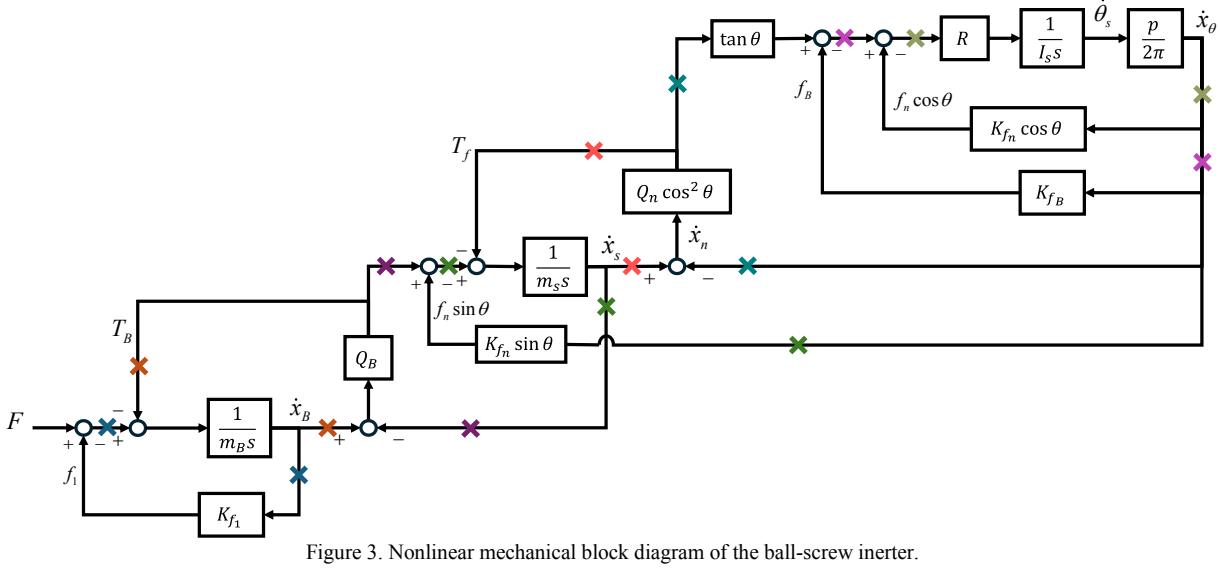

Figure 3. Nonlinear mechanical block diagram of the ball-screw inerter.

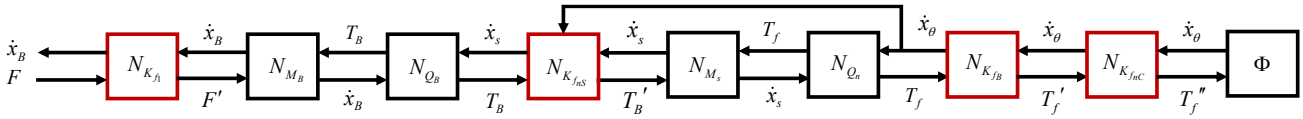

Figure 4. Two-port representation of the nonlinear ball-screw inerter.

Using the two-port representation, subsystems can be combined or bypassed. For example, Fig. 4 can be simplified as Fig. 5 if $f_n \sin\theta$ is relatively small and negligible. Suppose the stiffness and damping relationships are $Q_B = c_B + k_B / s$ and $Q_n = c_n + k_n / s$, we can further simplify the model as the equivalent network as shown in Fig. 6. Furthermore, the nonlinear model shown in Fig. 6 can be reduced to a linear model if all nonlinear blocks are neglected and bypassed in a well-lubricated situation, i.e., $K_{f_1} = K_{f_2} = 0$.

III. Experimental Verification

This section derives model parameters and verifies the proposed network by experiments. The inputs were sinusoidal displacements on the ungrounded terminal with frequencies of 0.5, 1, and 1.5 Hz. The force and acceleration were measured by load cells and accelerometers. We applied six small and two big flywheels to set the system's inertance, labeled A_1–A_6 and B_1–B_2, respectively. A_0 denotes the setting that no flywheel is attached to the ball screw. The theoretical inertance from A_0 to B_2 can provide a system inertance of 474.7–23261.4 kg, with a varying mass m_s of 15.4–30.2 kg by changing flywheels. For example, Fig. 7. Shows the experimental responses employing A_1.

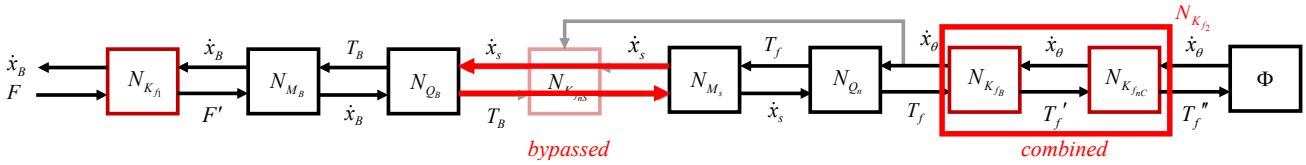

Figure 5. Reduced two-port network.

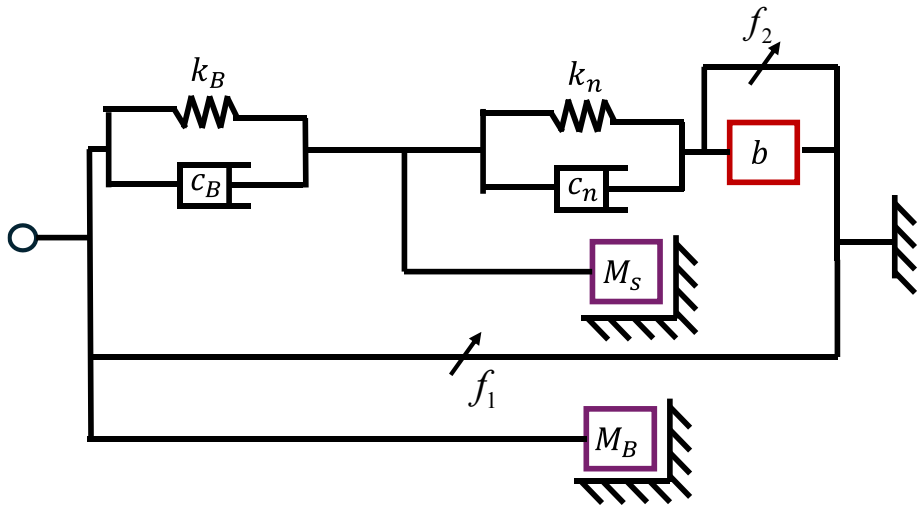

Figure 6. Equivalent mechanical network of the reduced two-port network.

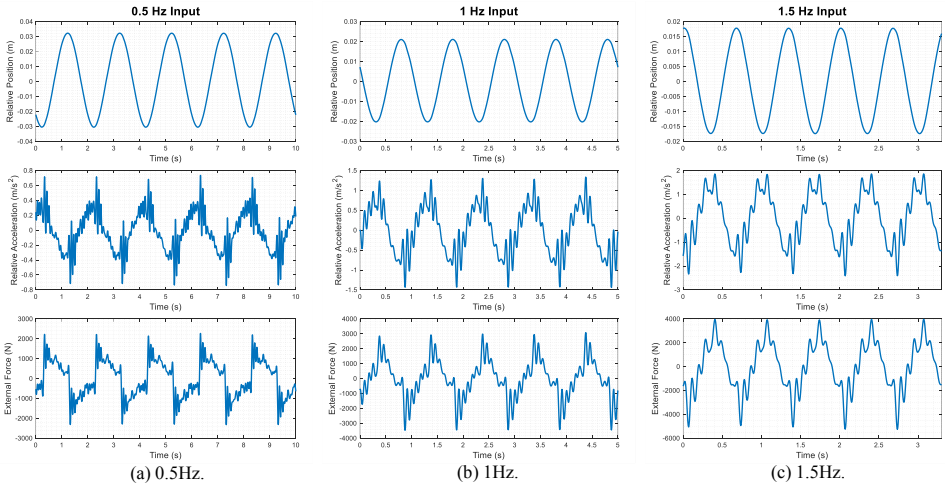

(a) 0.5Hz. (b) 1Hz. (c) 1.5Hz.

Figure 7. Experimental responses with flywheel A_1.

We tuned the parameters of the nonlinear network by iterations. For example, we applied the networks in Fig. 5 and Fig. 6 with the following friction models [12]:

$$\begin{aligned} f_1 &= f_{1,0}\,\mathrm{sgn}\left(\dot{x}_B\right)+c_{f_1}\dot{x}_B, \\ f_2 &= f_{2,0}\,\mathrm{sgn}\left(\dot{x}_\theta\right)+c_{f_2}\dot{x}_\theta, \end{aligned} \tag{3}$$

where $f_{1,0}$ and $f_{2,0}$ are the Coulomb friction forces, and c_{f_1} and c_{f_2} are the viscous friction force constants.

A nonlinear model was built in Simscape for simulation. Suppose that the measured forces are the network input and the acceleration is the network output, we applied the following equation to derive model parameters:

$$\Omega = \arg\min_{\text{para.}} \frac{\left\|a_{est}(t)-a_m(t)\right\|_2}{\left\|a_m(t)-\bar{a}_m\right\|_2}, \tag{4}$$

where Ω is the optimal parameter set, including the strain effect $\left(c_B, k_B, c_n, k_n\right)$, frictions $\left(f_{1,0}, c_{f_1}, f_{2,0}, c_{f_2}\right)$, and inertance b. a_m is the measured relative acceleration, while a_{est} is the estimated acceleration by the model.

We define the following fitting accuracy φ to quantify the effectiveness of the model:

$$\varphi = \left(1-\frac{\left\|a_{est}(t)-a_m(t)\right\|_2}{\left\|a_m(t)-\bar{a}_m\right\|_2}\right)\times 100\%. \tag{5}$$

Using the simplified network of Fig.5, the simulation can match the experimental responses with an average fitting accuracy of around 75%, 10% better than the nonlinear model in [12] and 26% better than the linear model. Fig. 8 compares the simulation and experimental results using flywheels A1

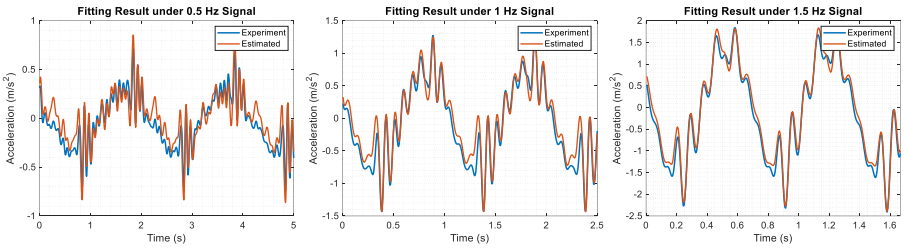

(a) with flywheel, A1.

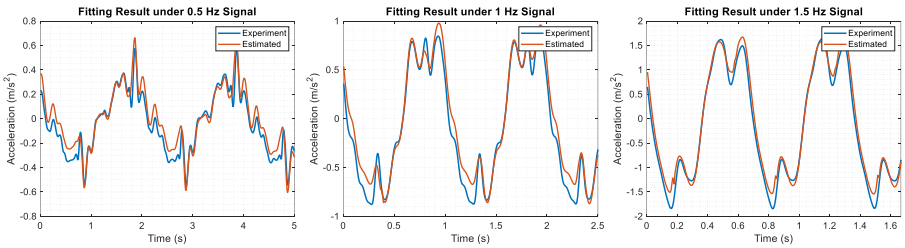

(b) with combined flywheels, A6.

Figure 8. Fitting results.

TABLE 1. PARAMETER SET OF THE NONLINEAR MODEL.

Tuned Parameters	**Value**
Damping Coefficient c_n	2165100 Ns/m
Stiffness Coefficient k_n	434960 N/m
Damping Coefficient c_B	1.0026 Ns/m
Stiffness Coefficient k_B	64015000 N/m
Coulomb Friction $f_{1,0}$	731.66 N
Viscous Friction c_{f_1}	0.027520 Ns/m
Coulomb Friction $f_{2,0}$	2.7780 N
Viscous Friction c_{f_2}	1574.7 Ns/m
Device Parameters	**Value**
Mass of Terminal 1 m_B (Iron Plate + Bearing + 2 × Ball Spline Nut)	57.200 kg
Mass of Small Flywheel ($\phi 0.19 \times 0.009m$)	2.09418 kg
Mass of Big Flywheel ($\phi 0.35 \times 0.009m$)	7.41836 kg
Mass of Ball Screw	15.406 kg

and A6 at three frequencies, while Table 1 illustrates the tuned and device parameters.

Table 2 shows the fitting results, while Fig. 9 compares the theoretical and the derived inertances. Based on these results, the proposed models can capture the dynamics of the ball-screw inerter device in practical working situations.

IV. Conclusion

This paper has proposed a two-port representation for the ball-screw inerter employing nonlinear characteristics. We derived a nonlinear model and conducted experiments for verification. The proposed model can represent the ball-screw inerter dynamics during operations based on the results. Additional nonlinear effects or mechanical characteristics can be considered in the future to predict system responses. This work lays the foundation for future research when designing mechanical systems employing the inerter.

Acknowledgment

The authors appreciate Professor Mi-Ching Tsai of National Cheng-Kung University for his theoretical guidance and NCREE for helping the experiments.

References

[1] M. C. Smith, "Synthesis of mechanical networks: The inerter," (in English), *IEEE Transactions on Automatic Control,* Article vol. 47, no. 10, pp. 1648-1662, 2002, doi: 10.1109/TAC.2002.803532.

[2] M. C. Smith and F.-C. Wang, "Performance Benefits in Passive Vehicle Suspensions Employing Inerters," in *Proceedings of the IEEE Conference on Decision and Control*, 2003, vol. 3: Institute of Electrical and Electronics Engineers Inc., pp. 2258-2263.

[3] F.-C. Wang and M.-K. Liao, "The lateral stability of train suspension systems employing inerters," *Vehicle System Dynamics,* vol. 48, no. 5, pp. 619-643, 2010.

[4] F.-C. Wang and S.-Y. Wu, "Vibration control of an optical table employing mechatronic inerter networks," *Journal of vibration and control,* vol. 22, no. 1, pp. 224-234, 2016.

[5] A. A. Taflanidis, A. Giaralis, and D. Patsialis, "Multi-objective optimal design of inerter-based vibration absorbers for earthquake protection of multi-storey building structures," *Journal of the Franklin Institute,* vol. 356, no. 14, pp. 7754-7784, 2019/09/01/ 2019, doi: https://doi.org/10.1016/j.jfranklin.2019.02.022.

[6] D. Pietrosanti, M. De Angelis, and A. Giaralis, "Experimental study and numerical modeling of nonlinear dynamic response of SDOF system equipped with tuned mass damper inerter (TMDI) tested on shaking table under harmonic excitation," *International Journal of Mechanical Sciences,* vol. 184, p. 105762, 2020/10/15/ 2020, doi: https://doi.org/10.1016/j.ijmecsci.2020.105762.

[7] F.-C. Wang, M.-F. Hong, and T.-C. Lin, "Designing and testing a hydraulic inerter," *Proceedings of the Institution of Mechanical Engineers, Part C: Journal of Mechanical Engineering Science,* vol. 225, no. 1, pp. 66-72, 2011.

[8] F.-C. Wang and W.-J. Su, "Impact of inerter nonlinearities on vehicle suspension control," *Vehicle system dynamics,* vol. 46, no. 7, pp. 575-595, 2008.

[9] L. Yuehao, C. Zhe, H. Niaoqing, Y. Yi, and X. Zhuo, "Modeling, design and experiments of a ball-screw inerter with mechanical diodes," *Journal of Sound and Vibration,* vol. 504, p. 116121, 2021/07/21/ 2021, doi: https://doi.org/10.1016/j.jsv.2021.116121.

[10] X. Q. Sun, L. Chen, S. H. Wang, X. L. Zhang, and X. F. Yang, "Performance investigation of vehicle suspension system with nonlinear ball-screw inerter," (in English), *Int. J. Automot. Technol.,* Article vol. 17, no. 3, pp. 399-408, 2016, doi: 10.1007/s12239-016-0041-x.

[11] Z. Li, K. Xu, K. Bi, Q. Han, and X. Du, "Inerter Nonlinearity and Its Influence on Control Efficiency of TMDI for Suppressing Vortex-Induced Vibration of Bridges," (in English), *J Bridge Eng,* Article vol. 27, no. 11, 2022, Art no. 04022101, doi: 10.1061/(ASCE)BE.1943-5592.0001941.

[12] J. Song, K. Bi, R. Ma, Z. Wang, K. Xu, and H. Hao, "Vibration control of adjacent structures equipped with inerter-based dampers considering nonlinearities: Analytical and experimental studies," *Mechanical Systems and Signal Processing,* vol. 206, p. 110903, 2024/01/01/ 2024, doi: https://doi.org/10.1016/j.ymssp.2023.110903.

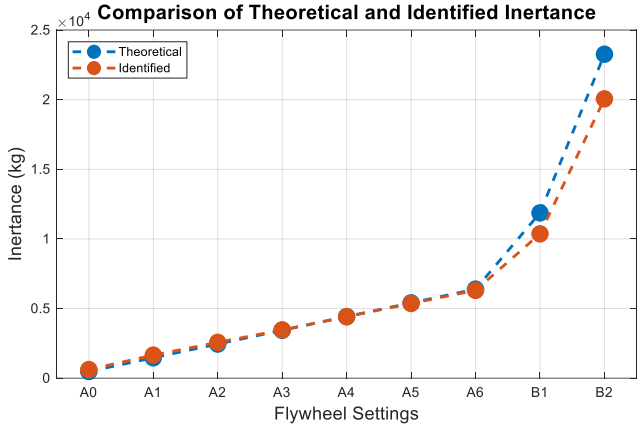

Figure 9. Comparison of the theoretical and tuned inertances.

TABLE 2. FITTING RESULTS OF THE NONLINEAR MODEL UNDER DIFFERENT FLYWHEEL SETTINGS AND INPUTS.

Flywheel Settings		**A_0**	**A_1**	**A_2**	**A_3**	**A_4**	**A_5**	**A_6**	**B_1**	**B_2**
	m_s (kg)	15.406	17.500	19.594	21.688	23.782	25.877	27.971	22.8	30.2
	IDed Inertance b (kg)	753.34	1668.9	2619.6	3531.6	4493.1	5461.5	6404.6	10468	20287
Fitting	0.5 Hz	6.6%	58.7%	66.4%	66.9%	69.7%	64.4%	68.3%	69.4%	68.2%
	1 Hz	52.3%	77.4%	82.9%	83.9%	85.8%	82.3%	81.8%	82.7%	77.6%
	1.5 Hz	74.3%	88.6%	90.3%	89.2%	89.2%	88.8%	88.0%	85.8%	84.5%